Journal of Photochemistry and Photobiology A: Chemistry 207 (2009) 20–27

Contents lists available at ScienceDirect

Journal of Photochemistry and Photobiology A: Chemistry

journal homepage: www.elsevier.com/locate/jphotochem

AFM-correlated CSM-coupled Raman and fluorescence properties of water-soluble oxo-titanium (IV) porphyrin bound with DNA

Ki. Seok Jeon[a,b], Tae Sook Park[a], Yung Doug Suh[b], Minjoong Yoon[a,*]

[a] Molecular/Nano Photochemistry & Photonics Lab, Department of Chemistry, Chungnam National University, Daejeon 305-764, Republic of Korea
[b] Advanced Materials Division, Korea Research Institute of Chemical Technology (KRICT), P.O. BOX 107, Yuseong, Daejeon, Republic of Korea

ARTICLE INFO

Article history:
Available online 20 January 2009

Dedicated to Professor Haruo Inoue on the occasion of his 60th birthday.

Keywords:
Atomic force microscopy (AFM)
Confocal scanning microscopy (CSM)
Raman/fluorescence spectroscopy
DNA–porphyrin interaction
Oxo-titanylporphyrin
Single DNA
Morphology
Excited-state charge transfer
Base pair dependence

ABSTRACT

The Raman and fluorescence spectroscopic properties of water-soluble oxo-titanium (IV) meso-tetrakis (1-methyl pyridium-4-yl) porphyrin (O=Ti(TMPyP)$^{4+}$) bound with calf thymus DNA and artificial DNAs such as double stranded poly[d(A-T)$_2$] and poly[d(G-C)$_2$] have been investigated on the single DNA molecule basis by atomic force microscopy (AFM)-correlated confocal scanning microscope (CSM)-coupled Raman and fluorescence spectroscopic techniques as well as the ensemble-averaged spectroscopy. The ensemble-averaged spectroscopic studies imply that the porphyrin interacts with DNA in different groove binding patterns depending on the base pairs. AFM-images of the different DNAs bound with O=Ti(TMPyP)$^{4+}$ were measured, and their morphologies are found to depend on kind of base pairs interacting with O=Ti(TMPyP)$^{4+}$. Being correlated with the AFM images, the CSM-coupled Raman and fluorescence spectral properties of the three different single O=Ti(TMPyP)$^{4+}$–DNA complexes were observed to be highly resolved and sensitive to base pair-dependent axial ligation of Ti–O bond as compared to the corresponding ensemble-averaged spectral properties, which affect the groove binding and its strength of the O=Ti(TMPyP)$^{4+}$ with DNA. The axial ligation was found to be accompanied by vibration structural change of the porphyrin ring, leading to keep the shape of double stranded poly[d(A-T)$_2$] rigid while poly[d(G-C)$_2$] and calf thymus DNA flexible after binding with the oxo-titanyl porphyrin. The base pair dependence of the fluorescence decay times of the DNA-bound porphyrins was also observed, implying that an excited-state charge transfer takes place in the G-C rich major groove in calf thymus DNA. These results suggest that binding of O=Ti(TMPyP)$^{4+}$ is more preferential with the G-C rich major groove than with the A-T rich minor groove in calf thymus DNA so that the morphology of DNA is changed.

1. Introduction

Since Fiel et al.'s discovery of intercalations of water soluble porphyrins into B-form DNA [1], numerous studies on porphyrin complexes with DNA, extensive investigations of porphyrins have been performed to exploit their medical, biological, and photophysical applications [2–5], on the basis of a good knowledge of their physicochemical properties. Particularly, some water-soluble cationic metalloporphyrins such as Au(III), Pt(II), Pd(II), and other heavy metal derivatives of H_2(TMPyP)$^{4+}$ are proved to be of interest in many areas as probes of the local DNA structure and dynamics [6,7], as artificial nucleases, and as possible DNA photosensitizers to be used in photodynamic therapy, and their interactions with DNA have been extensively investigated [8–11]. However, a number of questions for their interactions with DNA remain to be addressed unambiguously with respect to the following factors affecting the specific binding modes of the metalloporphyrins with DNA; the type, position and the charge number of substituent groups of the porphyrins, kinds and charges of metals, ionic strength of aqueous solution and the base-pair sequence of DNA. Particularly the porphyrin–DNA interaction effects on the DNA morphology changes and photophysical properties of the metalloporphyrins have not been clearly understood.

Furthermore, the interactions of oxo-metalloporphyrins with DNA have not been systematically studied as compared with other metallporphyrins, even though Raman studies of interaction between oxo-vanadyl porphyrins and DNA have been recently reported [12,13]. Therefore, the importance of accumulation of fundamental knowledge on interaction of water-soluble oxo-metalloporphyrins with DNA has been increasingly recognized, requiring various analytical tools. In this regard, resonance Raman spectroscopic techniques as well as NMR have been widely used together with the steady-state and time-resolved fluorescence spectroscopic techniques used for studying the photophysical

* Corresponding author. Tel.: +82 42 821 6546; fax: +82 823 7008.
E-mail address: mjyoon@cnu.ac.kr (M. Yoon).

1010-6030/$ – see front matter © 2009 Elsevier B.V. All rights reserved.
doi:10.1016/j.jphotochem.2009.01.005

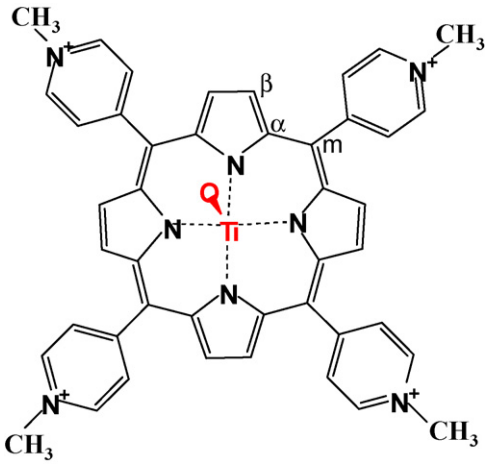

Scheme 1.

properties of metalloporphyrins with respect to their interactions with DNA. Nevertheless, the conventional Raman/fluorescence spectra are measured in large volume of solution which contains free porphyrins as well as porphyrin-bound DNA, based on ensemble-averaged measurements in spite of heterogeneity of DNA morphology. Thus, the conventional spectroscopic techniques result in the heterogeneous band broadening inherently, causing low frequency resolution to lose detail information of the molecular interactions with respect to morphology changes of DNAs bound with porphyrins [14]. Also they require strong laser power which can damage the sample. In order to solve these problems, it is necessary to detect the Raman or fluorescence signals of the porphyrins bound with DNA on the individual single DNA molecule basis with correlation to their morphologies.

Hereby, in this study, the atomic force microscope (AFM)-correlated confocal scanning microscope (CSM)-coupled Raman/fluorescence techniques were employed to investigate the interaction modes of the oxo-metalloporphyrins with single DNAs with respect to DNA morphology changes and photophysical properties. As a model metalloporphyrin, oxo-titanium meso-tetrakis (1-methyl pyridium-4-yl) porphyrin (O=Ti(TMPyP)$^{4+}$) (Scheme 1) was used with various DNAs such as double-stranded poly[d(A-T)$_2$], poly[d(G-C)$_2$] polynucleotides and calf thymus DNA. The oxo-titanyl porphyrins are the very rare truly mononuclear complexes of the oxo-titanyl ion (TiO^{2+}) [15], and they are classified as highly fluorescent porphyrins as compared to other metalloporphyrins and oxo-vanadyl porphyrins. Nevertheless, few studies have been done on their structures and vibrational spectral properties of the oxo-titanyl derivatives except recent theoretical [16] and X-ray crystallographic studies [17,18]. The Ti–O bond strength is affected by the axial ligation of the coordinating solvents due to the *trans* influence of the multiply bound oxide ligand as in the case of V–O bond [19,20]. However, the axial ligation of water has been suspected in contrast to the oxo-vanadyl porphyrins [21], even though the axial ligation is more feasible by the less protic solvents as observed by the protic solvent dependence of their fluorescence quantum yields ($0.2 > \varphi_f > 10^{-3}$) [22]. Less protic solvent forms relatively stable exciplex between solvent and porphyrin by the feasible six coordinated solvent ligation to the central metal, leading to formation of the excited M–L (d, π) charge transfer state which can be a precursor of electron donor [23]. Thus, these peculiar protic solvent effects of the photophysical properties make the oxo-titanylporphyrins to be useful as biological probes and photodynamic sensitizers, and it is interesting to pursue systematic studies on the biological environment effects on the structural and photophysical properties of this molecule.

2. Experimental

2.1. Chemicals and sample preparation

O=Ti(TMPyP)$^{4+}$ was purchased from the Porphyrin Products (Logan, Utah), and poly[d(A-T)$_2$], poly[d(G-C)$_2$] and calf thymus DNA were obtained from Amersham Biosciences. Each DNA was used without further purification. The sample solutions were prepared in an aqueous silver colloidal solution at pH 7 adjusted by phosphate buffer at room temperature. Ionic strength of phosphate buffer was adjusted to 0.1 M by addition of sodium chloride. For the resonance Raman measurements, silver colloids were added to the sample solutions. The DNA concentration was determined by measuring the absorbance at 260 nm. In order to prepare the mixture solution of the porphyrins and DNAs, the porphyrin stock solution was added to DNA solution and kept standing for 30 min. The concentration ratio of the DNA/porphyrin ratio was adjusted to be *ca.* 40 with the final porphyrin concentration of 3 μM. The concentration of DNAs were determined by using molar absorptivity of each DNA; $\varepsilon^{254\,nm} = 1.68 \times 10^4\,M^{-1}\,cm^{-1}$ for poly[d(A-T)$_2$], $\varepsilon^{262\,nm} = 1.32 \times 10^4\,M^{-1}\,cm^{-1}$ for poly[d(G-C)$_2$], $\varepsilon^{260\,nm} = 1.31 \times 10^4\,M^{-1}\,cm^{-1}$ for calf thymus DNA based on the UV absorption spectral measurement.

Samples for the AFM-correlated LCSM-coupled Raman/fluorescence measurement were prepared by immobilizing porphyrin-bound DNA *via* spin-casting of a few μL of the DNA/porphyrin mixture-solution on a poly-L-lysine-coated slide cover glass. The cover glass was cleaned by sonicating for 1 h in ethanolamine/water (25/75 by volume) mixture solvent and rinsed with deionized water and then with methanol, and drying in a vacuum oven (60 °C) before using.

2.2. Ensemble-averaged spectral measurements

All the ensemble-averaged spectra of porphyrins were measured in the aqueous solution. Absorption and fluorescence emission spectra of porphyrins were measured, respectively using a Varian Cary 3 spectrophotometer and a SLM-Aminco 4800 spectrofluorometer which makes it possible to obtain corrected spectra using Rhodamine B as a quantum counter. The resonance Raman spectra were measured by photoexcitation with 442 nm light from CW diode laser (Model 24R12, MWK industry) as previously described [23]. The sample solution was flowed through a glass capillary tube at a rate sufficient enough to ensure that each laser excitation encounters a fresh sample. The Raman signals were collected with a single pass spectrograph (Acton Research 500i) equipped with a charge-coupled device (PILN/CCD 1152E).

Circular dichroism (CD) spectra of the porphyrin–nucleic acid complex were measured on a Jasco 815 spectropolarimeter. The signal was averaged over an appropriate number of scans.

2.3. AFM-correlated CSM-coupled Raman/fluorescence measurements

The AFM-correlated CSM-coupled Raman/fluorescence measurement systems were set-up by modifying nanoscale CSM-coupled Raman systems developed previously [24] as shown in Fig. 1. The AFM (Bioscope, Digital Instrument Inc., Veeco Metrology Group) using a Nanoscope IV controller, is mounted on a micro-mechanical stage as previously described [23]. The scanning confocal microscope is based on an inverted optical microscope (Axiovert, 135, Zeiss) and a piezoelectric X–Y sample scanner (Physik Instrument, Polytech) driven by an independent home-made scanning controller. The sample-coated cover slide glass on a scanning piezo-electric X–Y stage (Physik Instrumente, P517.3CL) was illuminated with 514.5 nm light (~10 μW/cm^2) from CW diode

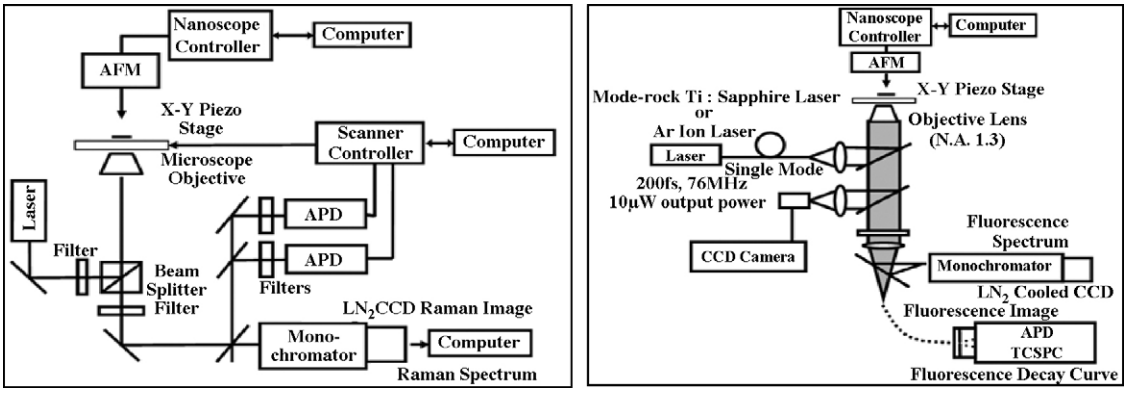

Fig. 1. Schematic diagram of ps-time-resolved AFM-correlated CSM-coupled Raman (left) and fluorescence (right) spectroscopic systems.

laser (Model 24R12, MWK industry) for Raman spectral measurement or second harmonic generated self-mode-locked Ti:sapphire laser (Coherent model Mira 900) (405 nm) pumped by a Nd:YVO_4 laser (Coherent Verdi diode pumped laser) (200 fs pulse width with repetition rate of 76 MHz) for fluorescence images, steady-state and time-resolved spectra measurements. The excitation light was passing through the single mode optic fiber and then incident on the back of a 100 × 1.3 NA oil immersion objective lens (Carl Zeiss Plan-NEOfluor). To collect Raman spectra, the scattered light after the beam-splitter is focused into the entrance slit (200 μm width) of a single-stage monochromator (Triax, 550, JovinYvon) by a 200-mm lens. The fluorescence signals were collected through an inverted confocal scanning microscope (Carl Zeiss Axiovert 200). The emission was isolated from Rayleigh scattering by a combination of filters, an excitation filter BP 395-440, a dichoric filter FT 460 and an emission filter LP 470 (Carl Zeiss). The fluorescence lifetimes were measured by using time-correlated single photon counting method with a self-mode-locked picosecond Ti–sapphire laser (Coherent Co.) pumped by Nd:YAG laser. This method allows a time resolution of about 20 ps after deconvolution.

3. Results and discussion

3.1. UV–vis absorption and CD spectral properties

Fig. 2(a) shows the UV–vis absorption spectra of O=Ti(TMPyP)$^{4+}$ measured in the presence of poly[d(A-T)$_2$], poly[d(G-C)$_2$] and calf thymus DNA, exhibiting the spectral changes of Soret band in the region of 436–443 nm and Q-band in the region of 550–610 nm, indicating interaction between O=Ti(TMPyP)$^{4+}$and the DNAs. The absorption maximum of the free porphyrin at 436 nm was observed to be substantially red shifted to 442 nm with a large hypochromicity upon interaction with poly[d(A-T)$_2$], whereas the red shift is not as large as that observed upon interaction with poly[d(G-C)$_2$] in spite of the hyperchromicity. Further, the absorption spectral changes with calf thymus DNA containing both G-C and A-T base pairs are more or less similar to that observed in the presence of poly[d(A-T)$_2$], indicating that the porphyrin interactions with DNA depend on the base pairs. It is also noteworthy that the positive CD spectra of the non-chiral O=Ti(TMPyP)$^{4+}$ were observed in the presence of the DNAs as shown in Fig. 2(b), confirming association of the porphyrin with DNA through the porphyrin's electronic transition dipole and the chiral DNA base pairs. The positive CD signal in the Soret region indicates that the interaction patterns of the O=Ti(TMPyP)$^{4+}$ with all the DNAs are similarly attributed to groove binding without any stacking or intercalation as in the case of oxovanadyl porphyrins bound with poly[d(A-T)$_2$] [13,25]. However, the positive CD spectral features depend on the kind of DNAs in parallel with the absorption spectral changes, again implying that the groove binding modes or strength of O=Ti(TMPyP)$^{4+}$ would depend on composition of the base pairs of DNAs.

3.2. Ensemble-averaged Raman/fluorescence spectral properties

In order to understand the binding modes in detail, in the first place, ensemble-averaged resonance Raman spectra of O=Ti(TMPyP)$^{4+}$ were measured in the absence and presence of different DNAs in the aqueous solution by excitation with 442 nm light (Fig. 3). The Raman bands are relatively broad, but readily

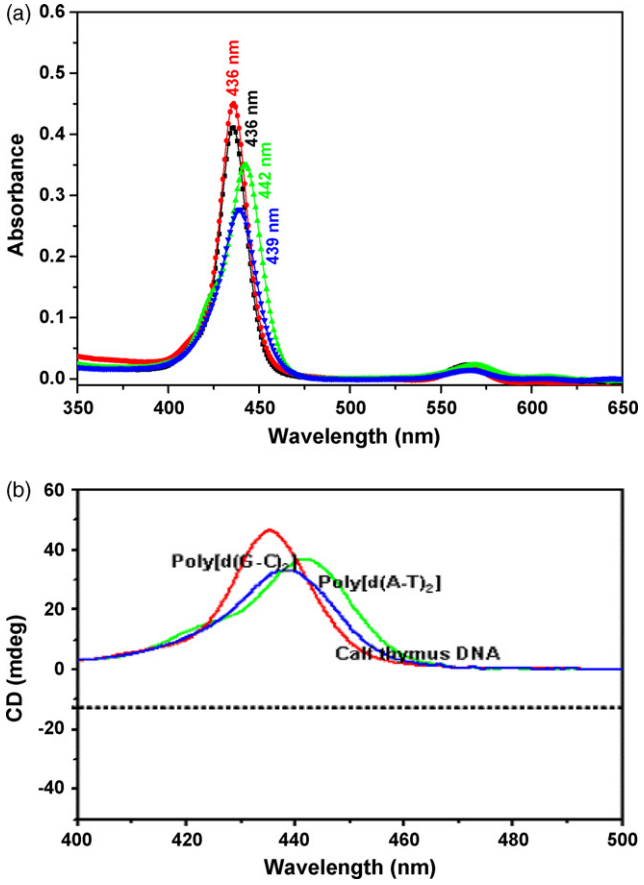

Fig. 2. (a) UV–vis absorption spectra of O=Ti(TMPyP)$^{4+}$ bound with various DNA in phosphate buffer solution containing silver colloids: (■) free; (●) poly[d(G-C)2]; (▲) poly[d(A-T)2]; (▼) calf thymus DNA. (b) Circular dichroism (CD) spectra of O=Ti(TMPyP)$^{4+}$measured in the presence of various DNA in the Soret absorption region. The base pairs/porphyrin ratio was *ca.* 40. The final porphyrin concentration was 3 μM.

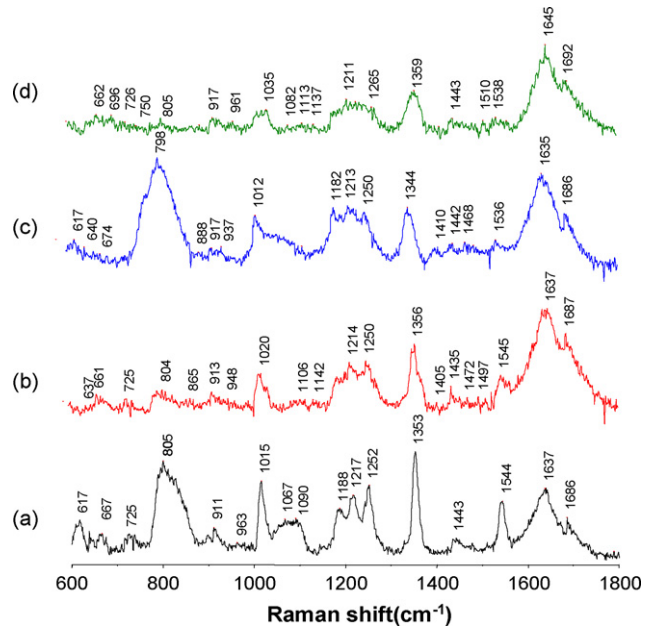

Fig. 3. Ensemble-averaged resonance Raman spectra of O=Ti(TMPyP)$^{4+}$ in the absence (a) and presence of (b) poly[d(G-C)$_2$], (c) poly[d(A-T)$_2$], and (d) calf thymus DNA in aqueous silver colloidal solution.

assigned with reference to the normal mode analysis of similar metallo-(TMPyP)$^{4+}$ [26–28] and other oxo-titanyl porphyrin [16] as listed in Table 1. The porphyrin macrocyclic bands of free O=Ti(TMPyP)$^{4+}$ are assigned as follows: the $\nu_2(C_\beta–C_\beta)$, $\nu_4(C_\alpha–N)$, and $\nu(C_\alpha–C_m)$ modes are assigned to the bands at 1544, 1353, and 1015 cm^{-1}, respectively. The pyridine bands are also observed: $\delta(C_m–Pyr)$ at 1252 cm^{-1}, δ(Pyr) at 1217 cm^{-1}, $\delta(Pyr)+\nu(N^+–CH_3)$ at 1188 cm^{-1} and $\nu(C–C)_{Pyr}+\nu(N^+–CH_3)$ at 805 cm^{-1}. These bands are similar to those observed from another oxo-metalloporphyrin, O=V(TMPyP)$^{4+}$ in terms of Raman shift and intensities [13,29]. On the other hand, the stretching band of Ti–O bond was observed around 1067 cm^{-1}, which is up-shifted as compared to that of V–O bond of the oxo-vanadyl porphyrin [13]. It is interesting to note that this stretching frequency is about the same as the theoretically calculated value [16]. Further, a water-ligated Ti–O stretching band ($\nu(OTi)\cdots(H_2O)$) was not observed even in the aqueous solution, implying that no six-coordinated adduct of coordinate O=Ti(TMPyP)$^{4+}$ exist in the aqueous solution in contrast to the case of O=V(TMPyP)$^{4+}$ as expected from the previous reports

Table 1
Ensemble-averaged Raman frequencies (cm^{-1}) and band assignments of free O=Ti(TMPyP)$^{4+}$ and its DNA complexes.

Assignment[a,b]	Free	Poly[d(G-C)$_2$]	Poly[d(A-T)$_2$]	Calf thymus DNA
Φ_4, δ(pyr)	1637	1637	1637	1640
ν_2, $\nu(C_\beta–C_\beta)$	1544	1545	1538	1538
ν_3, $\nu(C_\alpha–C_\beta)$	1472	1472	1468	1468
ν_4, $\nu(C_\alpha–N)$	1353	1354	1344	1349
ν_1, $\delta(C_m–pyr)$	1252	1250	1250	1255
δ(pyr)	1217	1214	1213	1211
$\delta(pyr)+\nu(N^+–CH_3)$	1188	1184	1182	1184
ν_9, $\delta(C_\beta–H)$	1090	1106	1106	1113
$\nu(OTi)\cdots(H_2O)$	–	–	–	–
$\nu(OTi)$[b]	1067	–	1060	–
ν_6, $\nu(C_\alpha–C_m)$	1015	1020	1012	1035
ν_7, $\delta(C–C)_{ph}$	911	913	913	915
$\nu(C–C)_{pyr}+\nu(N^+–CH_3)$	805	804	798	805

[a] Based on the reference to the normal mode analysis of similar metallo-(TMPyP)$^{4+}$s [26–28]. The following designations of the internal coordinates are used: ν-stretching, Φ-folding, δ-bending.

[b] Ref. [16].

[22]. This must be due to the stronger Ti–O bond than V–O. The Ti–O bond is considered to be resulted from more feasible σ-electron donor interaction between the filled O^{2-} p_z orbital and the empty Ti^{4+} d_z orbital, and π-electron donor interactions between the filled p_x and p_y orbitals and the empty d_{xz} and d_{yz} orbitals as compared to V–O bond. Thus, electron donation from water may not be competitive enough to have the *trans*-effect [30] in the oxo-titanyl porphyrins. Furthermore the Ti–O stretching band is relatively weak as compared to the corresponding V–O stretching mode [13]. This might be due to a small variation of the bond dipole moment of Ti–O bond as compared to V–O with respect to the normal coordinate which results in low polarizability variation around Ti–O bond. If this is the case, a large polarizability variation would take place around the porphyrin ring and pyridine bonds, as supported by the relatively higher intensity of the pyridyl bands (δ(Pyr) at 1637 cm^{-1} and $\nu(C–C)_{Pyr}+\nu(N^+–CH_3)$ at 805 cm^{-1}.

Most of the ensemble-averaged Raman bands measured in the presence of DNAs (Fig. 3(b–d)) were observed to exhibit band shifts and intensity variations due to the groove binding of the O=Ti(TMPyP)$^{4+}$ with DNA as expected from the absorption spectral studies. Particularly, the Ti–O stretching band of the free porphyrin complex at 1067 cm^{-1} is significantly down-shifted to overlap with the stretching band of ($C_\alpha–C_m$) at 1015 cm^{-1} upon interaction with the DNAs as shown in Fig. 3, indicating that the groove binding of the porphyrin with DNAs is accomplished by axial ligation of Ti–O with nitrogen at 7 position (N_7) of purine base of DNA. The intensity of the down-shifted Ti–O band is stronger in poly[d(A-T)$_2$] than in poly[d(G-C)$_2$] while it is intermediate in calf thymus DNA. This may be due to difference in the ligation ability of the different base pairs. Actually A-T base pair and G-C pair have two and three hydrogen-bonding, respectively, and the ligation ability of two hydrogen-bonding A-T base pair is expected to be stronger than that of three hydrogen-bonding G-C base pair as inferred from the fact that the axial ligation of protic solvent with Ti–O becomes stronger as the hydrogen bonding ability of the solvent increases [22]. Thus, the axial ligation of the porphyrin should be stronger in poly[d(A-T)$_2$] than in poly[d(G-C)$_2$] as expected from the absorption spectra. Such base-pair dependent Ti–O ligation would lead the porphyrin ring to interact with DNA base pairs differently. As expected, the intensities of the ν_2, ν_4, and $\nu(C_\alpha–C_m)$ bands are obviously decreased in the presence of the DNAs in spite of slight band shifts, indicating that polarizability of the porphyrin ring is reduced by binding of the oxo-titanyl porphyrin with hydrophobic environment of DNAs. Interestingly, reduction of the band intensities was observed to be smaller in poly[d(A-T)$_2$] than in poly[d(G-C)$_2$] and calf thymus DNA, indicating that the porphyrin ring in poly[d(A-T)$_2$] still faces hydrophilic aqueous environment as compared to that in poly[d(G-C)$_2$] or calf thymus DNA. This observation suggests that the porphyrin ring is inserted further into the G-C rich major groove in calf thymus DNA even though the axial ligation with the G-C region is weaker than with A-T region. On the contrary, the porphyrin ring can be inserted into the wider major groove (G-C rich region). Consequently, the porphyrin ring vibration would be also affected differently depending on the base pairs of DNA. If this is the case, the DNA binding effects on vibration frequencies of the porphyrin ring bonds must be clearly observed, but it was difficult to identify the band shifts and band width change correctly because of the line broadening in the ensemble-averaged Raman spectra of the mixed state of free porphyrins and DNA-bound porphyrins. Also the vibration structural changes of the porphyrin ring bound with different DNAs are expected to affect the vibronic structures of the fluorescence spectra differently. Fig. 4 shows the vibronic structures of the ensemble-averaged fluorescence of the porphyrins in different aqueous DNA solutions were observed at 570, 610 and 670 nm, respectively for 0–0, 0–1 and 0–2 vibrations. However, the spectral features

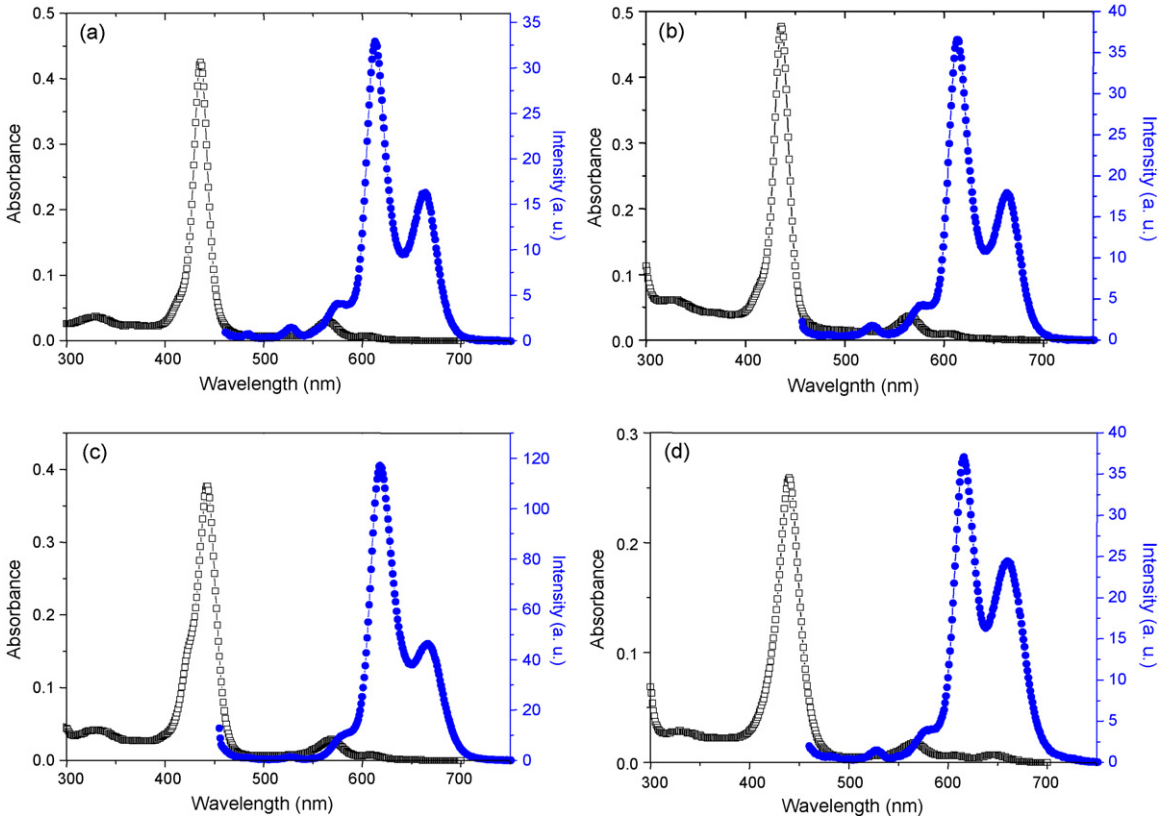

Fig. 4. Ensemble-averaged fluorescence spectra with absorption spectra of free O=Ti(TMPyP)$^{4+}$ (a), and O=Ti(TMPyP)$^{4+}$ bound with poly[d(G-C)$_2$] (b), poly[d(A-T)$_2$] (c) and calf thymus DNA (d) in aqueous solution. Excitation wavelength was 405 nm.

are almost the same due to the ensemble-averaged detection. Therefore, in order to study the vibration structural changes of the porphyrin ring more correctly, we tried to measure the Raman and fluorescence spectra of the single porphyrin-bound DNAs by using the AFM-correlated CSM-coupled Raman/fluorescence techniques.

3.3. *AFM-correlated CSM-coupled Raman/fluorescence spectral properties*

Fig. 5 shows the AFM-images of different DNAs bound with O=Ti(TMPyP)$^{4+}$ immobilized on cover glass, which exhibit double strand morphologies of about 1 μm length. Diameter of each DNA was determined to be 68, 74 and 70 nm, respectively for the oxo-titanyl porphyrin-bound poly[d(A-T)$_2$], poly[d(G-C)$_2$] and calf thymus DNA. The morphologies of DNAs seem to be changed upon binding with the O=Ti(TMPyP)$^{4+}$ as Takatoh et al. observed for DNA bound with 5,10,15,20-tetrakis[4-trimethylamminophenyl]porphyrin-tetra toluenes-4-sulfonate [14]. The shape of double strands of poly[d(A-T)$_2$] seems to be rigid while that of poly[d(G-C)$_2$] or calf thymus DNA looks more or less flexible after binding of the oxo-titanyl porphyrin. This may be due to the base-pair dependent binding modes and strength as discussed above. In order to confirm this, the Raman and fluorescence spectra of the oxo-titanyl porphyrin-bound DNA complexes were measured on a single DNA molecule basis by using the CSM-coupled Raman and fluorescence spectral system.

Fig. 6 shows the CSM-coupled Raman spectra of the single O=Ti(TMPyP)$^{4+}$-bound single DNAs selected from the AFM images and free oxo-titanyl porphyrin powders adsorbed on the quartz glass. In general, the CSM-coupled Raman spectra exhibit more highly resolved bands than the ensemble-averaged Raman spectra, and the vibration bands could be correctly assigned

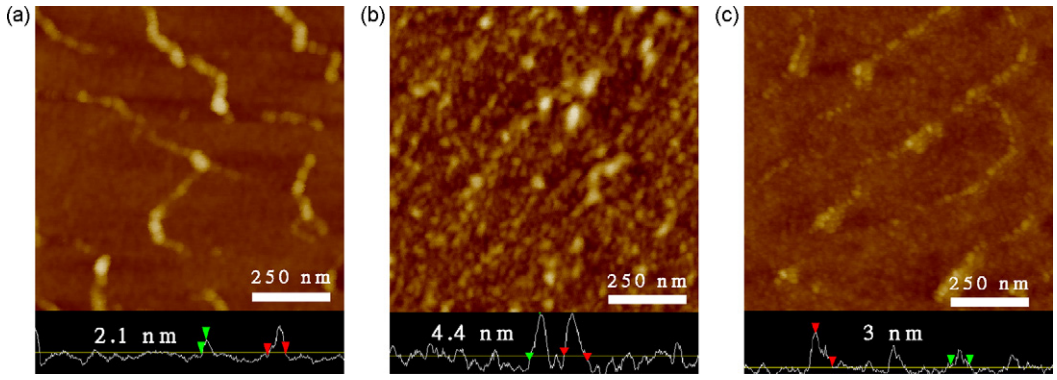

Fig. 5. AFM-images of different DNAs bound with O=Ti(TMPyP)$^{4+}$: (a) poly[d(A-T)$_2$], (b) poly[d(G-C)$_2$] and (c) calf thymus DNA immobilized on cover glass.

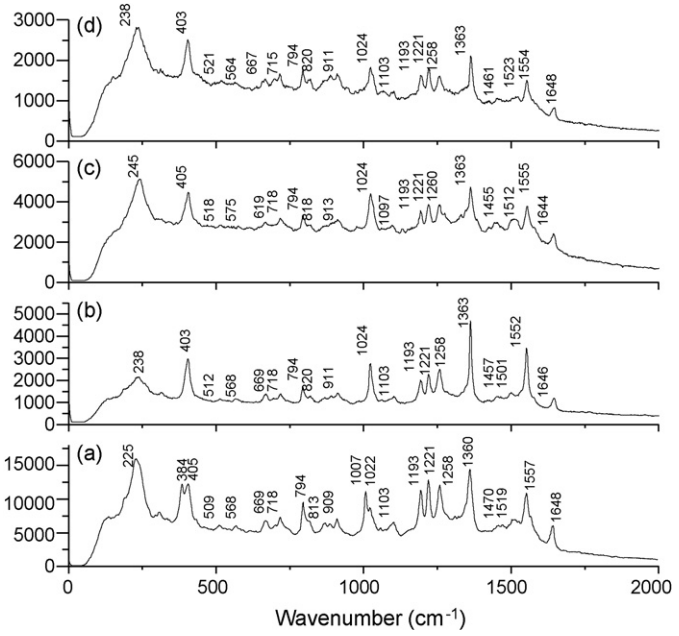

Fig. 6. AFM-correlated CSM-Raman spectra of free O=Ti(TMPyP)$^{4+}$ (a), and O=Ti(TMPyP)$^{4+}$ bound with poly[d(G-C)$_2$] (b), poly[d(A-T)$_2$] (c) and calf thymus DNA (d).

and listed in Table 2. The porphyrin macrocyclic bands of free O=Ti(TMPyP)$^{4+}$ (Fig. 6(a)) are more or less up-shifted as compared with those of the ensemble-averaged Raman bands as assigned as follows: the ν_2, and ν_4 modes are assigned to the bands at 1557 and 1360, respectively. The pyridine bands are also observed: $\delta(C_m–Pyr)$ at 1258 cm^{-1}, δ(Pyr) at 1221 cm^{-1}, δ(Pyr) + $\nu(N^+–CH_3)$ at 1193 cm^{-1}, and $\nu(C–C)_{Pyr} + \nu(N^+–CH_3)$ at 794 and 813 cm^{-1} which are resolved from the broad band at 805 cm^{-1} observed in the ensemble-averaged spectrum. This up-shift may be due to lack of water which interacts with the porphyrin ring bonds. On the other hand, the stretching band of Ti–O bond, which is not disturbed by water as described above, is significantly down-shifted to 1022 cm^{-1} from 1067 cm^{-1} measured in diluted aqueous solution, indicating that the highly concentrated oxo-titanyl porphyrins can be bound with each other by the axial ligation of Ti–O so that Ti–O bond strength is weakened. This intramolecular interaction in solid powder seems to cause the $\nu(C_\alpha–C_m)$ down-shifted to 1007 cm^{-1} from 1015 cm^{-1} observed in the aqueous solution.

Upon binding with DNAs, the Ti–O stretching band of the free oxo-titanyl porphyrins at 1022 cm^{-1} and one of the porphyrin ring bands, $\nu(C_\alpha–C_m)$ at 1007 cm^{-1} are merged into a single band at 1024 cm^{-1} as shown in Fig. 6(b–d). This may be due to removal of the intramolecular interaction of the oxo-titanyl porphyrin upon binding with the DNA base pairs. It is noteworthy that the 1024 cm^{-1} band of the poly[d(A-T)$_2$] or calf thymus DNA complex is broader than that of the poly[d(G-C)$_2$] complex, indicating the presence of the stronger axial ligation of Ti–O with A-T base pairs as observed from the ensemble-averaged Raman spectra. Such axial ligation of the Ti–O bond is accompanied by reduction of the Raman intensities of porphyrin ring bands from those of free oxo-titanyl porphyrins due to the less polar environments of the oxo-titanyl porphyrin in DNAs as discussed above. Such base-pair dependent Ti–O ligation would lead the porphyrin ring to interact with DNA base pairs differently. As expected, the intensities of the ν_2, ν_4, and $\nu(C_\alpha–C_m)$ bands are obviously decreased in the presence of the DNAs in spite of slight band shifts, confirming that the porphyrin ring faces less hydrophobic environment in poly[d(A-T)$_2$] than in poly[d(G-C)$_2$] and calf thymus DNA as predicted from the ensemble-averaged Raman spectra. Also vibration frequencies of the main porphyrin ring bands (ν_2, ν_4, and $\nu(C_\alpha–C_m)$) were more clearly observed to change differently upon binding with different DNAs as compared to those observed from the ensemble-averaged Raman spectra, indicating that the interaction of the porphyrin ring depends on the base pairs. Nevertheless, the frequencies and band width of the pyridyl-related bands including $\delta(C_m–Pyr)$ at 1258 cm^{-1}, δ(Pyr) at 1221 cm^{-1}, δ(Pyr) + $\nu(N^+–CH_3)$ at 1193 cm^{-1}, and $\nu(C–C)_{Pyr} + \nu(N^+–CH_3)$ at 794 and 813 cm^{-1} are little affected, indicating that interaction of the peripheral substituent group with DNA is not as strong as the major porphyrin ring. Interestingly the folding mode band of $N–C_\alpha–C_m–C_\alpha–N$ was observed at 225 cm^{-1} from the free oxo-titanyl porphyrin, and it was observed to be greatly up-shifted to 245 cm^{-1} with increased intensity in the poly[d(A-T)$_2$] complex as compared to that observed in the poly[d(G-C)$_2$] complex and calf thymus DNA. Also the double stretching modes of Ti–N bond were observed at 384 and 405 cm^{-1} from the free oxo-titanyl porphyrin, and they are merged into one single band (403 cm^{-1}) in the DNA complexes, indicating the loss of vibration energy. The intensity of 403 cm^{-1} band is stronger in the poly[d(A-T)$_2$] complex than in the poly[d(G-C)$_2$] complex and calf

Table 2
CSM-coupled Raman frequencies (cm^{-1}) and band assignments of free O=Ti(TMPyP)$^{4+}$ and its DNA complexes.

Assignment[a,b]	Free	Poly[d(G-C)$_2$]	Poly[d(A-T)$_2$]	Calf thymus DNA
Φ_4, δ(pyr)	1648	1646	1644	1648
ν_2, $\nu(C_\beta–C_\beta)$	1557	1552	1555	1554
ν_3, $\nu(C_\alpha–C_\beta)$	1470	1457	1455	1461
ν_4, $\nu(C_\alpha–N)$	1360	1363	1363	1363
ν_1, $\delta(C_m–pyr)$	1258	1258	1260	1258
δ(pyr)	1221	1221	1221	1221
δ(pyr) + $\nu(N^+–CH_3)$	1193	1193	1193	1193
ν_9, $\delta(C_\beta–H)$	1103	1103	1097	1103
ν(OTi)···(H_2O)	–	–	–	–
ν(OTi)	1022	1024	1024	1024
ν_6, $\nu(C_\alpha–C_m)$	1007	–	–	–
ν_7, $\delta(C–C)_{ph}$	909	911	913	911
$\nu(C–C)_{pyr} + \nu(N^+–CH_3)$	794	794	794	794
	813	820	818	820
ν(Ti–N)[b]	405 384	403	405	403
$\varphi(N–C_\alpha–C_m–C_\alpha–N)$[b]	225	238	245	238

[a] Based on the reference to the normal mode analysis of similar metallo-(TMPyP)$^{4+}$s [26–28]. The following designations of the internal coordinates are used: ν-stretching, Φ-folding, δ-bending.
[b] Ref. [16].

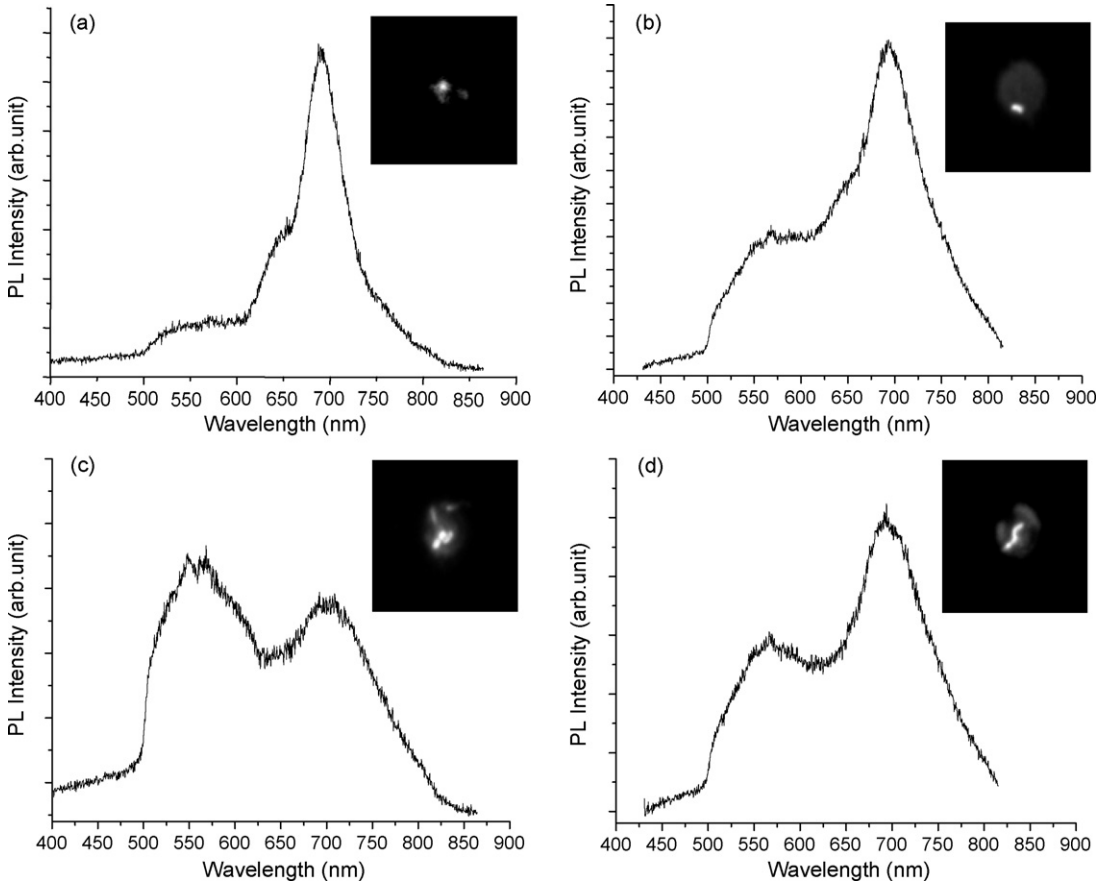

Fig. 7. AFM-correlated CSM-coupled fluorescence spectra of free O=Ti(TMPyP)$^{4+}$ (a) and O=Ti(TMPyP)$^{4+}$ bound with poly[d(G-C)$_2$] (b), poly[d(A-T)$_2$] (c) and calf thymus DNA (d). Each inset shows the fluorescence image of the single DNA bound with the porphyrins immobilized on quartz glass. Excitation wavelength was 405 nm.

thymus DNA, implying that O=Ti(TMPyP)$^{4+}$ is more loosely bound with the G-C rich region in DNA.

In order to confirm this and the DNA-binding effects on photophysical properties of O=Ti(TMPyP)$^{4+}$, the fluorescence spectra of different single DNA-bound O=Ti(TMPyP)$^{4+}$complexes were measured by the CSM-coupled fluorescence spectral system as shown in Fig. 7, and they were compared with those of free O=Ti(TMPyP)$^{4+}$ adsorbed on the quartz glass as the DNA-bound O=Ti(TMPyP)$^{4+}$complexes. Insets in the figure represent the fluorescence images of the single DNA-bound O=Ti(TMPyP)$^{4+}$complexes, exhibiting the morphologies of DNA strands as observed from the AFM images. The fluorescence of free oxo-titanyl porphyrin powder exhibits the 0–0, 0–1 and 0–2 vibronic emission bands respectively at 550 nm, 640 nm and 680 nm (Fig. 7(a)). The 0–0 and 0–1 emissions are quenched as compared to that of 0–2 emission by self-absorption due to high concentration in the powder state. However, these emissions are significantly enhanced in the DNA-complexes due to dilution of the oxo-titanyl porphyrin by binding with base pairs. The emission enhancement is the greatest in poly[d(A-T)$_2$] complex (Fig. 7(c)) whereas it is similar in both poly[d(G-C)$_2$] and calf thymus DNA complexes (Fig. 7(b and d)). This confirms that O=Ti(TMPyP)$^{4+}$ is bound preferably with the G-C rich region in calf thymus DNA. Nevertheless, the vibronic bands are not highly resolved in poly[d(A-T)$_2$] complex as compared to those in both poly[d(G-C)$_2$] and calf thymus DNA complexes, indicating that the porphyrin ring is deeply inserted into the G-C rich major groove in calf thymus DNA as discussed previously. Thus, DNA probably deforms after binding with porphyrin to access more hydrogen bonding environment.

We also measured the fluorescence lifetimes of the free oxo-titanyl porphyrin and its DNA complexes by monitoring two vibronic emission at 613 and 664 nm, and summarized in Table 3. The free oxo-titanyl porphyrin exhibits a single decay component with lifetime of 1.0 ns for both vibronic emissions, indicating that both emissions originates from the first electronically excited singlet state (S_1). However, in the poly[d(A-T)$_2$] complex, a long lifetime component (~9.0 ns) was observed in parallel with enhancement of the vibronic emission. This must be due to formation of the tightly bound complex with the A-T base pairs, which reduces vibration energy loss resulting in the inhibition of nonradiative

Table 3
Fluorescence lifetimes of the free O=Ti^{IV}(TMPyP)$^{4+}$ and its DNA complexes.

Samples	Wavelength			
	613 nm		664 nm	
	τ_{f1} (ns)	τ_{f2} (ns)	τ_{f1} (ns)	τ_{f2} (ns)
Free O=Ti(TMPyP)$^{4+}$	1.1 ± 0.1 (100%)	–	1.0 ± 0.1 (100%)	–
Poly[d(A-T)$_2$]-O=Ti(TMPyP)$^{4+}$	1.2 ± 0.2 (79%)	8.5 ± 0.3 (21%)	1.2 ± 0.2 (10%)	9.0 ± 0.3 (90%)
Poly[d(G-C)$_2$]-O=Ti(TMPyP)$^{4+}$	0.9 ± 0.1 (90%)	2.0 ± 0.2 (10%)	1.0 ± 0.1 (59%)	8.8 ± 0.2 (41.%)
Calf thymus DNA–O=Ti(TMPyP)$^{4+}$	1.0 ± 0.1 (34%)	2.0 ± 0.2 (66%)	1.0 ± 0.1 (69%)	2.3 ± 0.2 (31%)

transition. This long lifetime component is also observed in the poly[d(G-C)$_2$] complex, but its relative portion is decreased, indicating again that the oxo-titanyl porphyrin is loosely bound with the G-C base pairs. Instead, another new shorter lifetime component (~2.0 ns) was observed, implying that an excited charge transfer state of the oxo-titanyl porphyrin [22] may be formed more easily in the flexible G-C environment than in A-T environment because the G-C environment is less hydrophobic than the A-T as mentioned above. Such shorter lifetime component was also observed in the calf thymus DNA, supporting again that O=Ti(TMPyP)$^{4+}$ is bound with the G-C rich major groove than with the A-T rich minor groove.

4. Conclusion

The AFM images of the oxo-titanyl porphyrin–DNA complexes were measured, and their morphologies were observed to be different depending on kind of base pairs. Being correlated with the AFM images, the CSM Raman/fluorescence spectral properties of the single oxo-titanyl porphyrin–DNA complexes were observed to be sensitive to the base pair-dependent axial ligation with Ti–O bond and the ensuing vibration structural changes of porphyrin ring as compared to the ensemble-averaged spectral properties, demonstrating that the oxo-titanyl porphyrin is preferentially bound with G-C pair rich major groove than A-T rich minor groove in DNA so that the morphology of calf thymus DNA is changed. The nanoscale AFM-correlated CSM-coupled Raman/fluorescence spectroscopic properties of oxo-titanyl porphyrin–DNA interactions may be potential application in detection of single cancer cell.

Acknowledgements

This work is supported by the Korea Science Engineering Foundation (KOSEF R01-2004-000-10446-0), the Korea Research Foundation (KRF C00340) and "Development of Advanced Scientific Instrument" program funded by the Ministry of Education, Science and Technology.

References

[1] R.J. Fiel, J.C. Howard, E.N. Mark, N. Dattagupta, Nucleic Acids Res. 6 (1979) 3093.
[2] B. Jin, H.M. Lee, Y.-A. Lee, J.H. Ko, C. Kim, S.K. Kim, J. Am. Chem. Soc. 127 (2005) 2417.
[3] Y. Hiraku, K. Ito, K. Hirakawa, S. Kawanishi, Photochem. Photobiol. 83 (2007) 205.
[4] J.W. Winkleman, in: D. Kessel (Ed.), Advances in Experimental Medicine and Biology, 193, Plenum Press, New York, 1985, pp. 91–96.
[5] V.M. De Paoli, S.H. De Paoli, I.E. Borissevitch, A.C. edesco, J. Alloys Compd. 344 (2002) 27.
[6] J.W. Winkleman, J.H. Collins, Photochem. Photobiol. 46 (1987) 801.
[7] T. Akutsu, N. Yoshioka, H. Inoue, J. Biol. Inorg. Chem. 11 (2006) 527.
[8] M. Tabata, S.A. Kumar, E. Nyarko, J. Inorg. Biochem. 94 (2003) 50.
[9] E. Nyarko, N. Hanada, A. Habib, M. Tabata, Inorg. Chim. Acta 357 (2004) 739.
[10] S.N. Terekhov, V.S. Chirvony, P.-Y. Turpin, J. Appl. Spectrosc. 72 (2005) 585.
[11] P. Mojzes, S.G. Kruglik, V. Baumruk, P.-Y. Turpin, J. Phys. Chem. B 107 (2003) 7532.
[12] T.G. Park, J.H. Ko, A.Y. Ryoo, J.-M. Kim, D.W. Cho, S.K. Kim, Biochim. Biophys. Acta: Gen. Subjects 1760 (2006) 388.
[13] D.W. Cho, D.H. Jeong, J.-H. Ko, K.S. Kim, M. Yoon, J. Photochem. Photobiol. A: Chem. 174 (2005) 207.
[14] C. Takatoh, T. Masumoto, T. Kawai, T. Saitoh, K. Takeda, Chem. Lett. 35 (2006) 88.
[15] J.W. Buchler, in: D. Dolphin (Ed.), The Porphyrins, vol. I, Academic Press, New York, 1978, p. 435.
[16] A.V. Zakharov, G.V. Girichev, J. Mol. Struct.: THEOCHEM 851 (2008) 183.
[17] R. Guilard, J.-M. Latour, C. Lecomte, J.-C. Marchon, J. Protas, D. Ripoll, Inorg. Chem. 17 (1978) 1228.
[18] P.N. Dwyer, L. Puppe, J.W. Buchler, W.R. Scheidt, Inorg. Chem. 14 (1975 1782).
[19] M. Gouterman, R.A. Mathies, B.E. Smith, W.S. Caughey, J. Chem. Phys. 52 (1970) 3795.
[20] S.C. Jeoung, D. Kim, S.J. Hahn, S.Y. Ryu, M. Yoon, J. Phys. Chem. 102 (1998) 3795.
[21] S.S. Eaton, G.R. Eaton, J. Am. Chem. Soc. 97 (1975) 3660.
[22] S.Y. Ryu, M. Yoon, S.C. Jeong, N.W. Song, Photochem. Photobiol. Sci. 4 (2005) 54.
[23] S.C. Jeoung, D. Lim, D.W. Cho, M. Yoon, J. Phys. Chem. A 104 (2000) 4816.
[24] Y.D. Suh, G.K. Schenter, L. Zhu, P. Lu, Ultramicroscopy 97 (2003) 89.
[25] M. Lin, M. Lee, K.T. Yue, L.G. Marzilli, Inorg. Chem. 32 (1993) 3217.
[26] N. Blom, J. Odo, K. Nakamoto, D.P. Strommen, J. Phys. Chem. 90 (1986) 2647.
[27] J.S. Ha, O.-K. Song, M. Yoon, D. Kim, J. Raman Spectrosc. 21 (1990) 667.
[28] O.-K. Song, M. Yoon, D. Kim, J. Raman Spectrosc. 20 (1990) 739.
[29] Y.O. Su, R.S. Czernuszewicz, L.A. Miller, T.G. Spiro, J. Am. Chem. Soc. 100 (1988) 4150.
[30] J.W. Buchler, W. Kokisch, P.D. Smith, Struct. Bonding 34 (1978) 80.